Mineralogies and source regions of near-Earth asteroids

Tasha L. Dunn [a,*], Thomas H. Burbine [b], William F. Bottke Jr. [c], John P. Clark [a]

[a] Department of Geography-Geology, Illinois State University, Normal, IL 61790, United States
[b] Department of Astronomy, Mount Holyoke College, South Hadley, MA 01075, United States
[c] Southwest Research Institute, Boulder, CO 80302, United States

A B S T R A C T

Near-Earth Asteroids (NEAs) offer insight into a size range of objects that are not easily observed in the main asteroid belt. Previous studies on the diversity of the NEA population have relied primarily on modeling and statistical analysis to determine asteroid compositions. Olivine and pyroxene, the dominant minerals in most asteroids, have characteristic absorption features in the visible and near-infrared (VISNIR) wavelengths that can be used to determine their compositions and abundances. However, formulas previously used for deriving compositions do not work very well for ordinary chondrite assemblages. Because two-thirds of NEAs have ordinary chondrite-like spectral parameters, it is essential to determine accurate mineralogies. Here we determine the band area ratios and Band I centers of 72 NEAs with visible and near-infrared spectra and use new calibrations to derive the mineralogies 47 of these NEAs with ordinary chondrite-like spectral parameters. Our results indicate that the majority of NEAs have LL-chondrite mineralogies. This is consistent with results from previous studies but continues to be in conflict with the population of recovered ordinary chondrites, of which H chondrites are the most abundant. To look for potential correlations between asteroid size, composition, and source region, we use a dynamical model to determine the most probable source region of each NEA. Model results indicate that NEAs with LL chondrite mineralogies appear to be preferentially derived from the v_6 secular resonance. This supports the hypothesis that the Flora family, which lies near the v_6 resonance, is the source of the LL chondrites. With the exception of basaltic achondrites, NEAs with non-chondrite spectral parameters are slightly less likely to be derived from the v_6 resonance than NEAs with chondrite-like mineralogies. The population of NEAs with H, L, and LL chondrite mineralogies does not appear to be influenced by size, which would suggest that ordinary chondrites are not preferentially sourced from meter-sized objects due to Yarkovsky effect.

© 2012 Elsevier Inc. All rights reserved.

1. Introduction

The majority of asteroids orbit the Sun between Mars and Jupiter, in a region called the main asteroid belt. Many asteroids, however, have been ejected from the main asteroid belt and nudged into Earth-crossing orbits due to gravitational effects of other planetary bodies. These objects, called Near Earth Asteroids (NEAs), are of particular importance because of their close proximity to Earth and the consequent potential for a hazardous collision with our planet. Asteroids that are classified as NEAs have perihelion distances (q) $\leqslant$ 1.3 AU and aphelion distances (Q) $\geqslant$ 0.98 AU. To date, more than 8000 NEAs have been identified. Because most are relatively small (meters to kilometers in diameter), NEAs offer insight into a size range of objects that are not easily observed in the main asteroid belt. Of the 400 near-Earth asteroids that have been observed in the visible wavelength region, two-thirds have been classified as S- or Q-types (Binzel et al., 2004; Vernazza et al., 2008).

Both types are similar to the spectra of ordinary chondrites, the most common type of meteorite fall.

Several studies have attempted to determine the compositions and source regions of near Earth asteroids. Vernazza et al. (2008) used a radiative transfer model to analyze the spectra of 38 S- and Q-type NEAs from Binzel et al. (2006) and concluded that most NEAs have spectral properties similar to LL chondrites. They suggested that the Flora family (near the v_6 secular resonance) was the source region for NEAs with LL-like compositions. Thomas and Binzel (2010) used MGM (Modified Gaussian Modeling) to determine meteorite analogues for a sampling of NEAs and then used the Bottke et al. (2002a) dynamical model to determine the probable source region for each of those NEAs. They found that H chondrites have a higher than average delivery preference though the 3:1 mean motion resonance. de León et al. (2010) also concluded that the Flora family is the dominant source of NEAs and LL chondrites, based on inferred mineralogies of 72 NEAs.

These previous studies have relied primarily on modeling and statistical analysis to determine the composition of the NEA population. Though mineralogies of NEAs have been inferred from

spectral parameters (e.g. band area ratio vs. Band I center), they have not been calculated. Olivine and pyroxene, the dominant minerals in ordinary chondrites and many asteroids, have characteristic absorption features in the visible and near-infrared (VISNIR) wavelengths that can be used to determine their compositions and abundances. The primary diagnostic feature in olivine is a composite absorption feature at ~1 μm. Pyroxenes have two absorption bands at ~1 μm (Band I) and ~2 μm (Band II). The positions of both bands are sensitive to the compositions of olivine and pyroxene, moving to longer wavelengths as FeO increases (Adams, 1974; Burns et al., 1972; Cloutis, 1985). The combined absorption features near Band I and near Band II are also sensitive to the relative proportions of olivine and pyroxene. The ratio of Band II area to Band I area, called the band area ratio (BAR), is commonly used to estimate olivine and pyroxene abundances in meteorites and asteroids (Cloutis et al., 1986). The linear relationship between BAR and mafic mineral abundances was first recognized by Cloutis et al. (1986) and Gaffey et al. (2002) first developed calibrations for deriving olivine and pyroxene compositions from Band I and Band II center positions.

However, one problem with determining the mineralogies of NEAs is that formulas used previously for deriving pyroxene compositions (Gaffey et al., 2002) do not work very well for ordinary chondrite assemblages (Gaffey, 2007; McCoy et al., 2007). The Gaffey et al. (2002) formulas, which were derived using mixtures of olivine, low-Ca pyroxene, and high-Ca pyroxene, tend to calculate pyroxene mineralogies that are more Fe-rich than expected. This effect seems to be due the presence of three pyroxenes in ordinary chondrites (low-Ca pyroxene, high-Ca pyroxene, and pigeonite). Inaccurate NEA mineralogies can lead to misinterpretation of asteroid geologic histories. For example, Abell et al. (2007) suggested that Itokawa, the target of the Hayabusa mission, had experienced partial melting based on derived high-Fe content of pyroxene compositions. However, most other researchers argued that Itokawa's composition was similar to (unmelted) ordinary chondrites on the basis of its ground-based reflectance spectra (Binzel et al., 2001), Hayabusa reflectance spectra (Abe et al., 2006; Hiroi et al., 2006), and X-ray fluorescence data (Okada et al., 2006). Returned samples of Itokawa, which were LL-chondrite like in composition, confirmed its primitive origin (Nakamura, 2011).

Since two-thirds of NEAs have spectral parameters similar to ordinary chondrites, it is essential to accurately determine pyroxene and olivine compositions from VISNIR spectra. Dunn et al. (2010b) developed new formulas for deriving mineralogies of S-type and Q-type asteroids using ordinary chondrites powders originally prepared by Jarosewich (1990). Modal mineralogies of these powders were determined using X-ray diffraction and mineral compositions were measured using electron microprobe phase analysis (Dunn et al., 2010a). The derived formulas (with the corresponding R^2, the coefficient of determination) for determining the mineralogies of ordinary chondrite assemblages are:

$$ol/(ol + px) (\pm 0.03) = 0.242 * BAR + 0.728 \ (R^2 = 0.73) \qquad (1)$$

$$mol\% \ Fa \ in \ olivine \ (\pm 1.3) = -1284.9 * (BIC)^2 + 2656.5 * (BIC) - 1342.3 \ (R^2 = 0.92) \qquad (2)$$

$$mol\% \ Fs \ in \ pyroxene \ (\pm 1.4) = -879.1 * (BIC)^2 + 1824.9 * (BIC) - 921.7 \ (R^2 = 0.91) \qquad (3)$$

Because they are based on mineralogies of ordinary chondrites, these formulas provide a more accurate measure of asteroid with similar mineralogies (i.e. S-types and Q-types) than the formulas derived by Gaffey et al. (2002).

Here we provide an alternative method to previous studies, which used modeling and statistical analysis to characterize the NEA population, by calculating mineralogies of a sampling of meter- to kilometer-sized NEAs. Mineralogies derived using formulas from Dunn et al. (2010a) are extremely well-suited for S- and Q-type NEAs, which have mineralogies similar to ordinary chondrites (e.g., Gaffey et al., 1993). In addition, we implement the dynamic model of Bottke et al. (2002a) to determine the probable source region of each NEA. By combining derived mineralogies and source region probability, we can evaluate conclusions from previous studies, such the suggestion that the Flora family (near the v_6 secular resonance) is the source region for NEAs with LL chondrite-like compositions (Vernazza et al., 2008).

2. Data

We initially selected 138 NEAs with SpeX spectra that were visually similar to ordinary chondrites or reddened ordinary chondrites for analysis. The SpeX instrument (Rayner et al., 2003) is a medium-resolution cryogenic spectrograph located at the NASA Infrared Telescope Facility (IRTF) on Mauna Kea. SpeX can easily observe objects as faint as 17–18th magnitude, allowing high-quality near-infrared (0.8–2.5 μm) data (e.g., Binzel et al., 2001; Sunshine et al., 2004; Hardersen et al., 2004, 2005, 2006; Reddy et al., 2012a) to be obtained for relatively faint objects such as NEAs. Although the SpeX instrument is capable of producing reliable data down to 0.75 μm, SpeX data was collected with the dichoric filter in, which prevents acquisition of spectra at wavelengths shorter than 0.8 μm. Therefore, it is necessary to combine SpeX data with visible spectra (0.4–1.1 μm) from SMASS (small-main-belt asteroid survey) (Xu et al., 1995; Bus and Binzel, 2002a, 2002b) or Palomar (Binzel et al., 2001) to achieve full wavelength coverage between ~0.4 and ~2.5 μm. Visible wavelength coverage was available for 40 of the NEAs initially selected. Full wavelength spectra for these NEAs were downloaded from the MIT–UH–IRTF Joint Campaign for NEO Reconnaissance website (http://www.smass.mit.edu/minus.html). Taxonomic classifications (DeMeo et al., 2009) of the NEAs from this study are listed in Appendix A. All forty NEAs were classified as S-types (including subtypes) or Q-types, except 3199 Nefertiti (K-type) and 1999 JD6 (Xe-type). The composition and taxonomy of 1999 JD6 has also been examined by Reddy et al. (2012a).

To broaden our data set, we utilized spectra from the de León et al. (2010) spectrographic survey, which was conducted beginning in August 2002. de León et al. (2010) obtained visible and/or near-infrared spectra of 79 NEAs using telescopes at the El Roque de los Muchachos Observatory in the Canary Islands. We refer the reader to de León et al. (2010) for a detailed description of their observation campaign and data reduction techniques. de León et al. (2010) did not limit their analysis to S-type and Q-type asteroids, so their spectra represent a much broader range of asteroid types than the 40 NEAs selected from the MIT–UH–IRTF campaign. We selected 32 NEAs from de León et al. (2010) for which both visible and near-infrared spectra were available, bringing our total number of NEAs to 72. Most NEAs from de León et al. (2010) are S- or Q-type asteroids, but some V-types are included as well (Bus and Binzel, 2002a,b). Orbital elements, diameters, and taxonomic classification of all NEAs are presented in Appendix A (online supplemental). The observational conditions of the de León asteroids are provided in Appendix A4 of de León et al. (2010).

3. Spectral parameters

To determine asteroid mineralogies and modal abundances, we must first calculate Band I center (BIC) and BAR. Spectral parameters and standard deviations of the 40 NEAs from MIT–UH–IRTF

survey are listed in Table 1. Eleven of the NEAs, marked with an asterisk in Table 1, were observed on multiple dates. For these asteroids, the data in Table 1 represent the average values of all observations. Data for each individual observation is presented in Appendix B (online supplemental). Spectral parameters of the 32 NEAs from de León et al. (2010), which were determined as part of that study, are listed in Table 2.

Band area ratios were calculated using the trapezoidal rule. Using this technique, the area of each band is determined by calculating the area under a straight line tangent to the two reflectance peaks and then subtracting from it the area under the curve. The BAR is then calculated by dividing the area of Band II by the area of Band I. We calculated an average BAR for each NEA by randomly resampling each reflectance value 999 times using a Gaussian distribution for the given uncertainty at each reflectance point. The uncertainty of each BAR is the standard deviation of the 999 resampled BARs. Standard deviations of BARs ranged from 0.01 to 0.16, though 0.16 was anomalously high (Table 1). The mean uncertainty for all BARs was 0.02. We calculated Band I centers using the method of Storm et al. (2007). In this method, the continuum is divided out and then a second-degree polynomial is fit over the bottom third of each band. Band centers are then determined by visually identifying the center of the band. Following the procedure for BARs, the reflectance values for each spectrum were randomly resampled 999 times to determine an average Band I center. The mean uncertainty for all Band I centers was 0.003.

3.1. Surface temperature effects

Several studies have shown that band centers and BARs are influenced by changes in surface temperatures (Singer and Roush, 1985; Roush and Singer, 1987; Hinrichs et al., 1999; Moroz et al., 2000; Burbine et al., 2001). Moroz et al. (2000) demonstrated that BARs for olivine–pyroxene assemblages tend to increase at lower temperatures, such as the temperatures calculated for many NEAs ($\sim$200–300 K). Band center is affected by temperature as well, with the direction of movement of the Band I center depending on the percentage of olivine in the sample. To account for surface temperatures on NEAs, we corrected all BARs and Band I centers for temperature following procedures outlined in Burbine et al. (2009). We first estimated the surface temperatures (T) (K) for all NEAs using the following equation:

$$T = [(1 - A)L_o / 16\eta\varepsilon\sigma\pi r^2]^{1/4} \tag{4}$$

where A is the albedo, L_o is the solar luminosity (3.84×10^{26} W), η is the beaming factor (assumed to be unity) (e.g. Cohen et al., 1998), ε is the infrared emissivity (assumed to be 0.9), σ is the Stefan Boltzman constant (5.67×10^{-8} J s^{-1} m^{-2} K^{-4}), and r is the asteroid's distance from the Sun in meters. The asteroid's distance from the Sun at the time of observation was calculated using the Minor Planet center website (http://www.minorplanetcenter.net/iau/MPEph/MPEph.html). Since albedo of most NEAs is unknown, we used average albedos of each taxonomic class (S – 0.26, Q – 0.29, and V

Table 1
Calculated surface temperatures, Band I centers and uncertainties, band area ratios and uncertainties, and temperature corrections for each 40 NEAs from the MIT–UH–IRTF survey.

Asteroid		Surface temp. (K)	Band area ratio	ST DEV	Temp. correction	Band I center	St. dev.	Temp. correction
(433)	Eros[a]	216	0.527	0.008	−0.07	0.991	0.001	0.000
(719)	Albert	237	0.793	0.016	−0.05	0.985	0.001	0.000
(1620)	Geographos[a]	239	0.408	0.009	−0.05	0.997	0.002	0.000
(1627)	Ivar[a]	200	0.341	0.014	−0.08	0.978	0.002	0.000
(1685)	Toro	189	0.362	0.037	−0.09	0.984	0.003	−0.001
(1862)	Apollo[a]	257	0.243	0.004	−0.04	0.990	0.001	0.000
(1864)	Daedalus	193	0.624	0.020	−0.08	0.986	0.006	0.000
(1916)	Boreas	235	0.642	0.016	−0.05	0.985	0.002	0.000
(1943)	Anteros	198	0.768	0.029	−0.08	1.004	0.003	0.000
(1980)	Tezcatlipoca	246	0.262	0.010	−0.05	0.965	0.000	0.000
(3102)	Krok	226	0.874	0.019	−0.06	1.002	0.003	0.000
(3199)	Nefertiti[a]	204	0.063	0.017	−0.08	1.069	0.003	0.000
(3288)	Seleucus[a]	263	0.578	0.068	−0.03	1.007	0.004	0.000
(3753)	Cruithne	244	0.442	0.014	−0.05	0.972	0.006	0.000
(4179)	Toutatis[a]	242	0.643	0.010	−0.05	0.968	0.002	0.000
(5143)	Heracles	300	0.267	0.012	−0.01	1.007	0.003	0.000
(5587)	1990 SB	217	1.168	0.030	−0.07	0.933	0.003	0.000
(5660)	1974 MA	228	0.327	0.014	−0.06	1.020	0.003	0.000
(6239)	Minos	242	0.242	0.008	−0.05	0.988	0.003	0.000
(7336)	Saunders	241	0.298	0.013	−0.05	1.006	0.003	0.000
(7341)	1991 VK[a]	237	0.398	0.027	−0.05	0.996	0.003	0.000
(7482)	1994 PC$_1$	215	0.323	0.017	−0.07	1.012	0.004	0.000
(16960)	1998 QS$_{52}$[a]	217	0.647	0.021	−0.07	0.943	0.002	0.000
(18736)	1998 NU	241	0.894	0.075	−0.05	0.958	0.004	0.000
(20790)	2000 SE45	237	1.853	0.058	−0.05	0.945	0.005	0.000
(24475)	2000 VN$_2$	214	0.893	0.040	−0.07	0.971	0.003	0.000
(35107)	1991 VH[a]	243	0.378	0.018	−0.05	1.008	0.003	0.000
(53435)	1999 VM$_{40}$	241	2.137	0.070	−0.05	0.931	0.002	0.000
(66146)	1998 TU$_3$[a]	253	0.339	0.012	−0.04	0.994	0.003	0.000
(85989)	1999 JD$_6$	244	0.021	0.002	−0.05	1.106	0.006	0.000
(86819)	2000 GK$_{137}$	234	0.297	0.038	−0.05	0.986	0.008	0.000
(89355)	2001 VS$_{78}$	236	1.278	0.047	−0.05	0.932	0.004	0.000
(98943)	2001 CC$_{21}$	248	1.678	0.155	−0.04	1.025	0.029	0.000
(99907)	1989 VA	257	0.787	0.016	−0.04	0.936	0.002	0.000
(99942)	Apophis	263	0.527	0.063	−0.03	1.013	0.010	0.001
(138258)	2000 GD$_2$	258	0.478	0.022	−0.04	0.992	0.006	0.000
(138524)	2000 OJ$_8$	229	1.157	0.061	−0.06	0.930	0.001	0.000
(139622)	2001 QQ$_{142}$	256	0.491	0.049	−0.04	1.010	0.004	0.000
(162781)	2000 XL$_{44}$	235	1.284	0.101	−0.06	1.008	0.005	0.000
(200840)	2001 XN$_{254}$	261	0.535	0.030	−0.04	0.961	0.003	0.001

[a] The values for these asteroids are averages of multiple observations. Detail for each observation date is provided in Appendix A.

T.L. Dunn et al./Icarus 222 (2013) 273–282

Table 2
Calculated surface temperatures, Band I centers and uncertainties, band area ratios and uncertainties, and temperature corrections for 32 NEAs from de León et al. (2010).

Asteroid		Surface temp. (K)	Band area ratio	St. dev.	Temp. correction	Band I center	St. dev.	Temp. correction
(1036)	Ganymed	145	1.219	0.020	−0.12	0.915	0.005	−0.001
(1866)	Sisyphus	180	0.116	0.034	−0.09	0.950	0.004	−0.001
(3122)	Florence	206	0.463	0.034	−0.07	1.013	0.010	0.000
(3752)	Camillo	197	1.541	0.071	−0.08	0.943	0.009	0.000
(3908)	Nyx	228	2.254	0.005	−0.06	0.935	0.005	0.000
(4055)	Magellan	184	2.212	0.075	−0.09	0.930	0.005	0.000
(5626)	1991 FE	223	0.644	0.055	−0.06	0.926	0.001	0.000
(5653)	Camarillo	228	1.970	0.023	−0.06	0.920	0.005	0.000
(6047)	1991 TB1	225	2.086	0.158	−0.06	0.925	0.004	0.000
(6611)	1993 VW	179	1.647	0.226	−0.09	0.932	0.007	−0.001
(13553)	Masaakikoyama	241	1.454	0.247	−0.05	0.903	0.004	0.000
(21088)	1992 BL$_2$	232	0.237	0.018	−0.06	1.034	0.001	0.000
(25143)	Itokawa	227	0.579	0.055	−0.06	0.996	0.010	0.000
(30825)	1990 TG$_1$	233	0.372	0.039	−0.06	0.990	0.005	0.000
(65803)	Didymos	234	0.524	0.107	−0.06	0.983	0.005	0.000
(66251)	1999 GJ$_2$	226	0.409	0.053	−0.05	0.969	0.006	0.000
(68346)	2001 KZ$_{66}$	223	0.611	0.276	−0.06	1.005	0.006	0.000
(68950)	2002 QF$_{15}$	235	0.546	0.116	−0.06	0.950	0.005	0.000
(85867)	1999 BY$_9$	221	0.256	0.106	−0.07	1.006	0.005	0.000
(86039)	1999 NC$_{43}$	168	0.493	0.015	−0.10	0.961	0.003	−0.001
(88188)	2000 XH$_{44}$	213	1.783	0.011	−0.07	0.932	0.005	0.000
(136993)	1998 ST$_{49}$	143	0.593	0.069	−0.12	0.920	0.005	−0.001
(137427)	1999 TF$_{211}$	236	0.306	0.134	−0.05	0.960	0.005	0.000
(138846)	2000 VJ$_{61}$	206	1.565	0.115	−0.07	0.947	0.004	0.000
(143624)	2003 HM$_{16}$	243	1.121	0.121	−0.05	0.931	0.013	0.000
(154347)	2002 XK$_4$	235	0.530	0.271	−0.05	0.968	0.010	0.000
(159857)	2004 LJ	228	1.250	0.057	−0.06	0.948	0.009	0.000
(162149)	1998 YQ$_{11}$	238	0.745	0.221	−0.05	0.980	0.005	0.000
(162483)	2000 PJ$_5$	244	0.532	0.115	−0.05	1.006	0.005	0.000
(253841)	2003 YG$_{118}$	192	1.670	0.265	−0.08	0.929	0.004	0.000
	2002 QA$_{22}$	247	0.271	0.069	−0.05	1.010	0.005	0.000
	2004 LU$_3$	250	2.072	0.076	−0.04	1.030	0.006	0.000

– 0.42) (Thomas, 2011). Surface temperatures for each NEA are listed in Table 1 (our study) and Table 2 (de León et al., 2010).

We then used data from Moroz et al. (2000) to estimate temperature corrections to Band I centers and BARs for each NEA. Moroz et al. (2000) measured the effect of temperature on wavelength position in two ordinary chondrites, Elenovka (L5) and Soko-Banja (LL4). Using data from both chondrites, we established a linear regression that predicts the relationship between temperature and BAR and between temperature and Band I center position. The formulas for the temperature correction of BARs are:

$$\text{BAR correction} = 0.0009 \times T(\text{K}) - 0.2666$$
$$(\text{from LL chondrite, Soko-Banja}) \quad (5)$$

and

$$\text{BAR correction} = 0.0005 \times T(\text{K}) - 0.1708$$
$$(\text{from L chondrite, Elenovka}) \quad (6)$$

The formulas for the temperature correction of Band I center (BIC) wavelength position are:

$$\text{BIC correction} = 0.000078 \times T(\text{K}) - 0.2194$$
$$(\text{from LL chondrite, Soko-Banja}) \quad (7)$$

and

$$\text{BIC correction} = -0.000048 \times T(\text{K}) + 0.01512$$
$$(\text{from L chondrite, Elenovka}) \quad (8)$$

To determine the correction factor for band are ratio, we averaged the values from Eqs. (5) and (6) and the added this value from the calculated band are ratio of each asteroid. This process was repeated for the Band I center correction using Eqs. (7) and (8). However, because the effect of temperature change on Band I position was opposite in each chondrite (i.e. wavelength position decreased

with decreasing temperature in Elenovka and increased in Soko-Banja), the negative correction from the LL chondrite negated the positive correction from the L chondrite. This is not unexpected, since the direction of movement in Band I center varies depending on the percentage of olivine, and LL chondrites are more olivine-rich than L chondrites (48–52 wt.% vs. 38–45 wt.%) (Dunn et al., 2010a). As a result, a temperature correction was not required for the Band I center position in most asteroids (Tables 1 and 2). This minor temperature correction for Band I center is consistent with previous studies (e.g. Burbine et al., 2009), in which the correction due to temperature was <0.001 μm for Band I. The correction for band are ratio was more significant than Band I center position but still relatively minimal, as corrected values were typically 10–20% lower than the original BARs (Tables 1 and 2). Temperature corrections from this study are identical to those from Sanchez et al. (2012), as both sets of corrections were calibrated using ordinary chondrite data from Moroz et al. (2000).

3.2. Space weathering effects

Space weathering (e.g., Hapke, 2001) is a general term for the processes that can potentially alter the spectral properties of an "airless" body, such as interaction with galactic and solar cosmic rays, irradiation by solar wind particles, and micrometeorite impacts. These processes have been shown to darken the surface and redden the spectral slope through the production of nanophase iron (e.g., Pieters et al., 1993, 2000; Chapman, 1996; Hiroi and Sasaki, 2001; Sasaki et al., 2001). Attempts to quantify the effects of space weathering have focused primarily on S-and Q-type asteroids because of their relationship with ordinary chondrites. Spectra of Q-type asteroids match those of ordinary chondrites and therefore represent unweathered asteroid surfaces (McFadden et al., 1985; Bus, 1999). Q-type spectra that experience space weathering processes redden and darken to match S-type spectra (Binzel et al.,

2004, 1996; Chapman 1996; Sunshine et al., 1993). Though asteroid spectra become darker and redder as a result of space weathering, laboratory studies have shown that spectral parameters remain unchanged (Marchie et al., 2005; Sasaki et al., 2001), so interpreted mineralogies should not be affected (Vernazza et al., 2008; Sanchez et al., 2012).

3.3. Phase angle effects

Band parameters can also be affected by phase angle (g) – the angular separation of the Sun and the observer as seen by the target. Changes in phase angle are exhibited as phase reddening, which may make it difficult to discriminate phase angle effects from those of space weathering. However, phase angle-induced effects a have been observed in the laboratory (Gradie and Veverka, 1980; Reddy et al., 2012b) and confirmed by spacecraft observations of Eros (Clark et al., 2002), Itokawa (Abe et al., 2006), and Vesta (Reddy et al., 2012b). Sanchez et al. (2012) endeavored to quantify the effects of phase angle by analyzing VISNIR spectra of 12 S- and Q-type NEAs observed at various phase angles and three ordinary chondrites measured in the laboratory at phase angles from 13° to 120°. Though Sanchez et al. (2012) observed an increase in band depths and spectral slope with increasing phase angle, their results showed that the changes in spectral parameters with increasing phase angle were negligible. The largest shift in band center was ~0.01 μm and the largest variation in BAR was ~0.02, both of which are on the order of the error. Therefore, phase angle-induced effects on band parameters should have no significant impact on interpreted mineralogies.

4. Asteroid mineralogies

BARs and Band I centers have been used to determine probable meteorite analogues for asteroids since Gaffey et al. (1993) characterized the spectral parameters of the ordinary chondrites, basaltic achondrites, and olivine meteorites. Since then, spectral studies of primitive achondrites (Hiroi and Takeda, 1991; Burbine et al., 2001, 2006) and ureilites (Cloutis et al., 2010) have broadened the usage spectral parameters as tool for determining meteorite analogues from VISNIR asteroid spectra. In BAR vs. Band I center space (Fig. 1a and b) the H, L, and LL ordinary chondrites form linear trends within restricted range of space known as the ordinary chondrite "boot" (Gaffey et al., 1993). The howardites, eucrites, and diogenites (HEDs), a clan of pyroxene-rich basaltic achondrites from Asteroid 4 Vesta (Consolmagno and Drake, 1977; Binzel and Xu, 1993; Thomas et al., 1997; Drake, 2001; Reddy, 2012c), are characterized by BARs > ~1.5 and Band I centers < ~0.97 μm due to the high abundance of pyroxene (Gaffey et al., 1993; Burbine et al., 2009; Mayne et al., 2009; Reddy et al., 2010). Lodranites and acapulcoites, partially melted mixtures of low-Ca pyroxene and olivine (McCoy et al., 2000), fall between the ordinary chondrite and basaltic achondrites regions or overlap the most pyroxene-rich ordinary chondrites (H chondrites). Ureilites, which contain ~10% interstitial carbon, metal, and sulfides (Mittlefehldt et al., 1998), have pyroxene and olivine absorption features that are subdued in strength relative to ordinary chondrites and tend to have BARs slightly lower than those in the ordinary chondrites (Cloutis et al., 2010). However, a few ureilites do fall in the ordinary chondrite region. F-type 2008 TC$_3$ that exploded in the atmosphere and rained fragments over the Sudan was found to have a ureilite composition based on analyses of the recovered samples (Jenniskens, 2009).

The most probable meteorite analogue for each NEA was determined by plotting measured spectral parameters in BAR vs. Band I center space and comparing those to the spectral parameters of
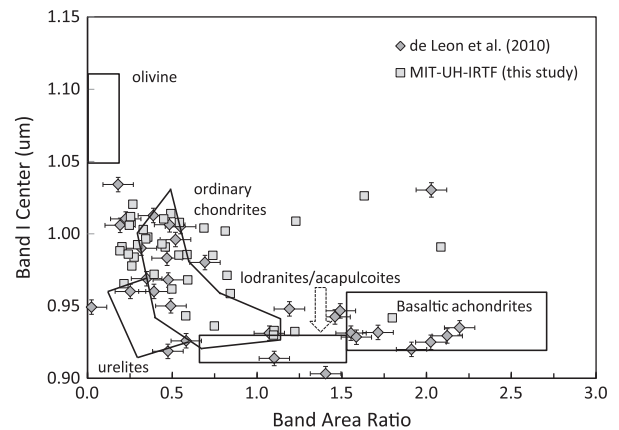

Fig. 1. Spectral parameters of 40 NEAs from the MIT–UH–IRTF survey (shown as squares) and 32 NEAs from de León et al. (2010) (shown as diamonds) plotted in terms of BAR vs. BIC. The primitive achondrite region (lodranites/acapulcoites) is from Burbine et al. (2001), the ureilite region is from Cloutis et al. (2010), and the olivine, ordinary chondrite, and basaltic achondrite regions are from Gaffey et al. (1993). As shown in Tables 1 and 2, uncertainty varies among spectra. For clarity, the error bars that are shown represents the average error. For our study, this error is within the size of the symbols, so no error bars are shown for the NEAs from this study.

known meteorite groups (as defined by regions shown in Fig. 1). Spectral parameters of all 72 NEAs are plotted on Fig. 1. NEAs from this study are represented by squares, while the NEAs from de León et al. (2010) are represented by diamonds. Of the 40 NEAs examined in this study, nineteen have spectral parameters consistent with ordinary chondrites, one has parameters that overlap between ordinary chondrites and the primitive achondrites region, and seven have analogues other than ordinary chondrites (two ureilites, two basaltic achondrites, two olivine meteorites, and one primitive achondrite). Asteroids (3199) Nefertiti and (85989) 1999 JD$_6$ have negative BARs, but both would be classified as olivine meteorites based on un-corrected BARs. Thirteen asteroids plot outside the regions defined by known meteorite groups, though only asteroids (162781) 2000 XL$_{44}$ and (98943) 2001 CC$_{21}$ do not appear to have a known meteorite analogue (Fig. 1). The remaining 11 NEAs plot in the immediate vicinity of the ordinary chondrite region. Though the error of the spectral parameters is such that these 11 NEAs are not classified as ordinary chondrites, their proximity to the ordinary chondrite region merits further consideration. Of the 32 NEAs from de León et al. (2010), nine have ordinary chondrite-like spectral parameters and four overlap between ordinary chondrites and another group (either primitive achondrites or ureilites). Twelve have analogues other than ordinary chondrites and seven are not consistent with any known analogue. Of those seven, three plot near the ordinary chondrite region. Table 3 lists the meteorite analogues for all 72 NEAs, as determined by BARs and Band I centers.

In total, 47 of the NEAs have spectra parameters that plot as ordinary chondrites, overlap between ordinary chondrites and another region, or plot just outside the ordinary chondrite region. Because these asteroids likely have like ordinary chondrite mineralogies, we can use the Dunn et al. (2010b) formulas derive their mineral abundances and compositions. These calibrations are valid for the compositional range of olivine and low-Ca pyroxene (Fa$_{15-34}$ and Fs$_{13-28}$) and the range of mineral abundances (ol/(ol + px) = ~0.45–0.70) found in ordinary chondrites (Brearley and Jones, 1998; Dunn et al., 2010a). The uncertainties of the values are 0.03 for ol/(ol + px), 1.3 mol% for Fa, and 1.4 mol% for Fs (Dunn et al., 2010b). Using the Dunn et al. (2010b) formulas, we calculated the abundance of olivine and pyroxene (as a ratio of ol/(ol + px)) and the composition of olivine (as mol% Fa) and

Table 3
Meteorite analogues of all 72 NEAs as determined using BAR and BIC.

	Asteroid	Meteorite analogue	Asteroid		Meteorite analogue	Asteroid		Meteorite analogue
(433)	Eros	OC	(5653)	Camarillo	BA	(85989)	1999 JD$_6$	Olv
(719)	Albert	OC?	(5660)	1974 MA	OC?	(86039)	1999 NC$_{43}$	OC or Ur
(1036)	Ganymed	PA	(6047)	1991 TB$_1$	BA	(86819)	2000 GK$_{137}$	OC?
(1620)	Geographos	OC	(6239)	Minos	OC?	(88188)	2000 XH$_{44}$	BA
(1627)	Ivar	OC?	(6611)	1993 VW	BA	(89355)	2001 VS$_{78}$	PA
(1685)	Toro	OC	(7336)	Saunders	OC?	(98943)	2001 CC$_{21}$	None
(1862)	Apollo	OC?	(7341)	1991 VK	OC	(99907)	1989 VA	OC
(1864)	Daedalus	OC	(7482)	1994 PC$_1$	OC?	(99942)	Apophis	OC
(1866)	Sisyphus	None	(13553)	Masaakikoyama	None	(136993)	1998 ST$_{49}$	Ur
(1916)	Boreas	OC	(16960)	1998 QS$_{52}$	OC	(137427)	1999 TF$_{211}$	Ur
(1943)	Anteros	Ur	(18736)	1998 NU	OC	(138258)	2000 GD$_2$	OC
(1980)	Tezcatlipoca	Ur	(20790)	2000 SE$_{45}$	BA	(138524)	2000 OJ$_8$	PA or OC
(3102)	Krok	OC?	(21088)	1992 BL$_2$	None	(138846)	2000 VJ$_{61}$	BA
(3122)	Florence	OC	(24475)	2000 VN$_2$	OC?	(139622)	2001 QQ$_{142}$	OC
(3199)	Nefertiti	Olv	(25143)	Itokawa	OC	(143624)	2003 HM$_{16}$	OC or BA
(3288)	Seleucus	OC	(30825)	1990 TG$_1$	OC	(154347)	2002 XK$_4$	OC
(3752)	Camillo	BA	(35107)	1991 VH$_1$	OC	(159857)	2004 LJ	OC?
(3753)	Cruithne	OC	(53435)	1999 VM$_{40}$	BA	(162149)	1998 YQ$_{11}$	OC
(3908)	Nyx	BA	(65803)	Didymos	OC	(162483)	2000 PJ$_5$	OC
(4055)	Magellan	BA	(66146)	1998 TU$_3$	OC	(162781)	2000 XL$_{44}$	None
(4179)	Toutatis	OC	(66251)	1999 GJ$_2$	OC or Ur	(200840)	2001 XN$_{254}$	OC
(5143)	Heracles	OC?	(68346)	2001 KZ$_{66}$	OC	(253841)	2003 YG$_{118}$	BA
(5587)	1990 SB	OC	(68950)	2002 QF$_{15}$	OC		2002 QA$_{22}$	OC?
(5626)	1991 FE	PA, OC, Ur	(85867)	1999 BY$_9$	OC?		2004 LU$_3$	None

Primitive achondrites (PA) (Burbine et al., 2001), ureilites (Ur) (Cloutis et al., 2010), and olivine meteorites (Olv), ordinary chondrites (OC), or basaltic achondrites (BA) (Gaffey et al., 1993); None – not consistent with any know analogue; OC? – plots near the OC region.

Table 4
Calculated mineralogies and ordinary chondrite analogues of the 47 NEAs with ordinary chondrite-like spectral parameters.

Asteroid		ol/(ol + px)	Fa	Fs	OC Type	Asteroid		ol/(ol + px)	Fa	Fs	OC type
(433)	Eros	0.62	28.3	23.4	LL	(25143)	Itokawa	0.60	28.9	23.8	LL
(719)	Albert	0.55	27.7	22.9	L/LL	(30825)	1990 TG$_1$	0.65	28.3	23.4	LL
(1620)	Geographos	0.64	29.1	23.9	LL	(35107)	1991 VH	0.65	29.5	24.2	LL
(1627)	Ivar	0.66	26.7	22.2	LL	(65803)	Didymos	0.61	27.5	22.7	L/LL
(1685)	Toro	0.66	27.6	22.8	LL	(66146)	1998 TU$_3$	0.66	28.6	23.5	LL
(1862)	Apollo	0.68	28.4	23.4	LL	(66251)	1999 GJ$_2$	0.64	25.4	21.2	L/LL
(1864)	Daedalus	0.60	27.7	22.9	LL	(68346)	2001 KZ$_{66}$	0.59	29.7	24.4	LL
(1916)	Boreas	0.59	27.8	23.0	LL	(68950)	2002 QF$_{15}$	0.61	21.8	18.6	L
(3102)	Krok	0.53	29.5	24.2	LL	(85867)	1999 BY$_9$	0.68	29.8	24.5	LL
(3122)	Florence	0.63	30.2	24.8	LL	(86039)	1999 NC$_{43}$	0.63	23.8	20.0	L
(3288)	Seleucus	0.60	29.8	24.5	LL	(86819)	2000 GK$_{137}$	0.67	27.8	23.0	LL
(3753)	Cruithne	0.63	25.8	21.5	L/LL	(99907)	1989 VA	0.55	18.5	16.2	H
(4179)	Toutatis	0.58	25.2	21.1	L/LL	(99942)	Apophis	0.61	30.3	24.9	LL
(5143)	Heracles	0.66	29.9	24.6	LL	(138258)	2000 GD$_2$	0.62	28.6	23.6	LL
(5587)	1990 SB	0.46	17.7	15.7	H	(138524)	2000 OJ$_8$	0.46	16.9	15.1	H
(5626)	1991 FE	0.59	15.8	14.3	H	(139622)	2001 QQ$_{142}$	0.62	30.1	24.7	LL
(5660)	1974 MA	0.66	30.5	25.1	LL	(143624)	2003 HM$_{16}$	0.47	17.3	15.4	H
(6239)	Minos	0.68	28.1	23.2	LL	(154347)	2002 XK$_4$	0.61	25.2	21.1	L/LL
(7336)	Saunders	0.67	29.8	24.5	LL	(159857)	2004 LJ	0.44	21.3	18.3	H
(7341)	1991 VK	0.64	29.0	23.8	LL	(162149)	1998 YQ11	0.56	27.1	24.5	L/LL
(7482)	1994 PC$_1$	0.67	30.1	24.8	LL	(162483)	2000 PJ$_5$	0.61	29.8	24.5	LL
(16960)	1998 QS$_{52}$	0.59	20.1	17.4	H	(200840)	2001 XN$_{254}$	0.61	24.1	20.2	L
(18736)	1998 NU	0.52	23.5	19.8	L		2002 QA$_{22}$	0.67	30.1	24.7	LL
(24475)	2000 VN$_2$	0.53	25.7	21.4	L						

The least root mean square errors are 0.03 for ol/(ol + px), 1.3 mol% for Fa, and 1.4 mol% for Fs (Dunn et al., 2010b).

low-Ca pyroxene (as mol% Fs) for these 47 NEAs (Table 4). Calculated mineralogies are consistent with measured ordinary chondrite mineralogies, with modal abundances ranging from 0.44 to 0.69 ol/(ol + px), olivine from Fa$_{15.3–30.5}$, and low-Ca pyroxene from Fs$_{14.0–24.9}$.

Using compositional regions for the H, L, and LL chondrites defined by Dunn et al. (2010b), we determined the best ordinary chondrite analogue (H, L, or LL) for each NEA (Table 4). Mineralogies are plotted as ol/(ol + px) vs. mol% Fa in Fig. 2a. and vs. mol% Fs in Fig. 2b. The NEAs with ordinary chondrite-like spectral parameters (including those that overlap another region) are represented by boxes, while the NEAs that plot just outside the ordin-

ary chondrite region are represented by diamonds. Based on derived Fa content of olivine (Fig. 2a), all of the NEAs with certain ordinary chondrite analogues are classified as H, L, or LL chondrites. The majority plot as LL chondrites and several have mineralogies that cannot be distinguished between the LL and L chondrites, due to compositional overlap between these regions. The results for Fs content in pyroxene (Fig. 2b) are nearly identical, with the only differences due to the extent of overlap between the L and LL regions. All NEAs that plot just outside the ordinary chondrite region are also classified as H, L, or LL ordinary chondrites when error of spectrally derived mineralogies is considered. All except for two are classified as LL chondrites based on Fa content
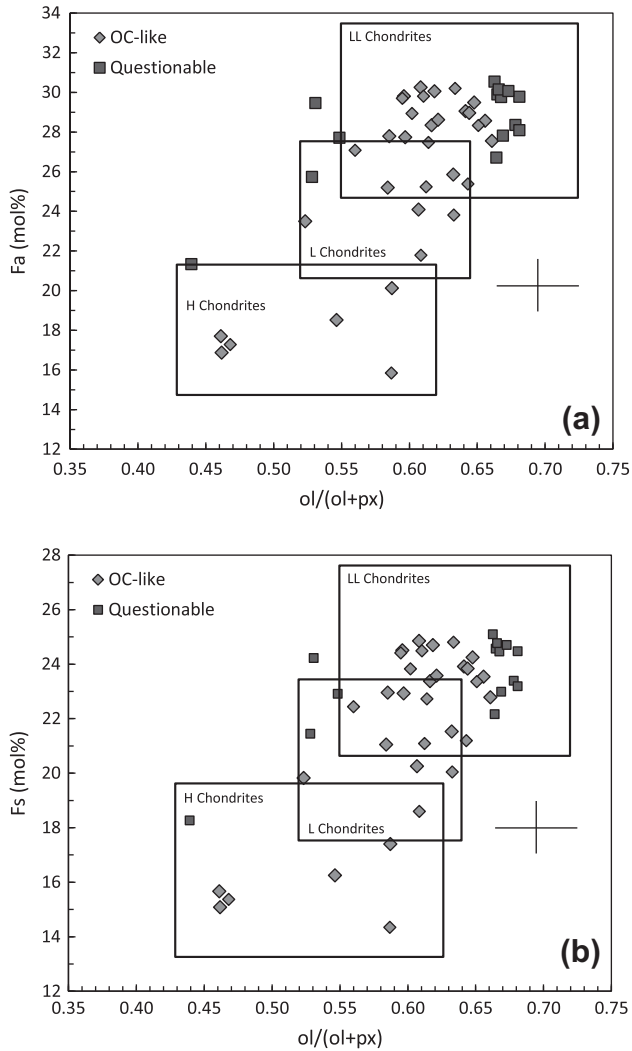
Fig. 2. Mineralogies the 47 NEAs with ordinary chondrite like BARs and BICs plotted as (a) ol/(ol + px vs. mol% Fa in olivine and (b) ol/(ol + px) vs. mol% Fs in low-Ca pyroxene. Compositional regions for the H, L, and LL chondrites were defined by Dunn et al. (2010b). NEAs with definitive ordinary chondrite-like spectral parameters are represented by boxes, while NEAs with questionable spectral classification are represented by diamonds. Error bars represent the least mean square error of spectrally derived mineralogies: 0.03 for ol/ol + px, 1.3 mol% Fa, and 1.4 mol% Fs.

Fig. 3. Distribution of the NEA source regions as determined using dynamical model designed by Bottke et al. (2002a) plotted in orbital parameter space as a function of semi-major axis (*a*) vs. eccentricity (*e*). The Bottke et al. (2002a) model determines the probability that an asteroid is derived from one of five primary source regions: the ν_6 secular resonance with Saturn, the intermediate source Mars-crossing region (IMC), the 3:1 mean motion resonance at 2.5 AU, the outer belt region (OB), and the Jupiter Family Comet region (JFC). Various mean-motion resonances are shown as dashed lines; the width of each resonance is not represented. The $i = 0°$ position of the ν_6 secular resonance is shown as a dashed line. The regions occupied by Apollos ($a \geqslant 1.0$ AU, $q \leqslant 1.0167$ AU), Atens ($a < 1.0$ AU, $Q \geqslant 0.983$ AU), and Amors (1.0167 AU $< q \leqslant 1.3$ AU) are labeled as such.
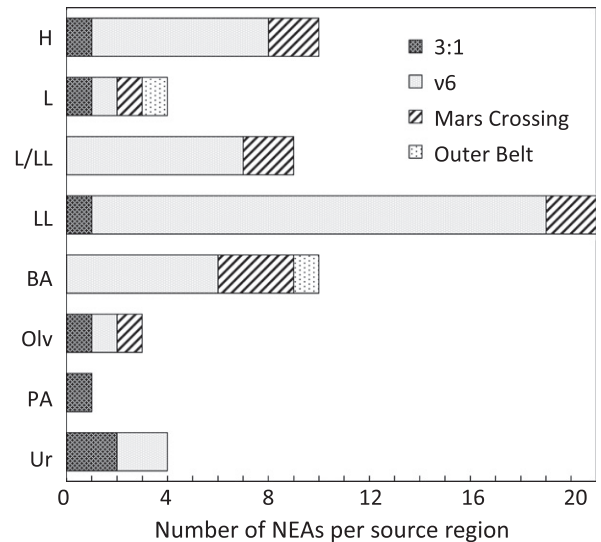

Fig. 4. Results from the Bottke et al. (2002a) model presented as asteroid mineralogy (likely meteorite analogue) vs. probable source region. Abbreviations for meteorite analogues are as follows: Primitive achondrites (PA), ureilites (Ur), olivine meteorites (Olv), and basaltic achondrites (BA). Ordinary chondrite groups are designated with H, L, LL, or L/LL.

(Fig. 2a). Based on their measured spectral parameters and their derived mineralogies, it is likely that these NEAs are ordinary chondrite-like in composition.

Overall, 15% of NEAs with ordinary chondrite analogues have H chondrite mineralogies, 10% have L chondrite mineralogies, 60% have LL chondrite mineralogies, and 15% have mineralogies that cannot be distinguished between L and LL chondrites. These abundances are consistent with results from previous studies, which indicate that the majority of NEAs have LL-chondrite mineralogies (Vernazza et al., 2008; de León et al., 2010). This, however, continues to be in conflict with the population of recovered ordinary chondrites, of which LL chondrites represent only 10%. Previous studies (Bottke et al., 2002b; Vernazza et al., 2008; Nesvorný et al., 2009) suggested that this discrepancy might be the result of different dynamical mechanisms or source regions for the NEA population and the meteorite population. One of the most probable mechanisms for delivering meteorites to Earth is the Yarkovsky effect (Bottke et al., 2002a, 2000; Rubincam 1995; Hartmann et al., 1999), which causes bodies to drift in orbital semi-major axis, thus increasing their potential to encounter resonances and be

delivered to the inner Solar System. The Yarkovsky effect transports meter-sized objects, such as those that supply the meteorite collection, more quickly than km-sized objects. Therefore, the compositional difference between the NEA population and the meteorite population may be due to the preferential delivery of meter-sized objects to the inner Solar System by the Yarkovsky effect.

To more closely examine the question of whether the contribution of chondrite material to planet crossing orbits becomes larger as one moves to smaller bodies, we examined the size distribution and mineralogies of the NEAs that were classified as H, L, or LL chondrites. We estimated the diameter of each NEA using the formula (Harris and Harris, 1997):

$$D = (1329 * 10^{-0.2H}) / \sqrt{p_V} \qquad (9)$$

where H is the absolute magnitude and p_V is the visual albedo. Absolute magnitudes were obtained from the Minor Planet Center website, and average albedos for each taxonomic class (Thomas, 2011) were used as approximate albedos for each NEA. Diameters of each NEA are listed in Appendix A. We then divided the OC-like NEAs into two size groups, those with diameters <1 km (20 NEAs) and those with diameters from 1 to 10 km (50 NEAs). The NEAs with diameters < 1 km represent a size range more likely to be the source of the meteorite collection. Two asteroids with diameters > 10 km were excluded from this analysis. We then calculated the percentages of NEAs with H, L, LL, and L/LL mineralogies within each group. Of the NEAs with diameters 1–10 km, 16% are H chondrites, 13% are L chondrites, 55% are LL chondrites, and 16% are either L or LL. The distribution within the <1000 m NEAS is comparable, with 15% H chondrites, 15% L chondrites, 46% LL chondrites, and 23% either L or LL chondrites. The distribution of mineralogies within the meter-sized NEAs is not consistent with proportions of H, L, and LL ordinary chondrites in the meteorite collection, which would appear to suggest that smaller bodies do not contribute material to planet-crossing orbits more readily than larger bodies. However, we have only analyzed a small proportion of the meter-sized NEA population and cannot make any broad conclusions from a small sampling.

5. Asteroid source regions

To determine if a relationship exists between NEA mineralogy and location in the inner Solar System, we used a dynamical model designed by Bottke et al. (2002a) to establish the source region of the NEAs examined in this study. The Bottke et al. (2002a) model determines the probability that an asteroid is derived from one of five primary source regions: the v_6 secular resonance with Saturn, the intermediate source Mars-crossing region (IMC), the 3:1 mean motion resonance at 2.5 AU, the outer belt region (OB), and the Jupiter Family Comet region (JFC). Orbital parameters used for the Bottke et al. (2002a) model are listed in Appendix A. Fig. 3 shows the distribution of NEAs in orbital parameter space as semi-major axis (a) vs. eccentricity (e). According to the source region model, most of our NEAs come from the innermost region of the main belt. Overall, 64% are derived from the v_6 resonance, 21% from the Mars crossing region, 11% from the 3:1 resonance, and 1% from the outer belt region. Two NEAs, 1992 BL$_2$ and 2002 QA$_{22}$, were outside of the model boundaries. Our results are consistent with those from de León et al. (2010) but differ from the predictions of Bottke et al. (2002a), who suggested that 37% of NEAs with absolute magnitudes $H < 22$ would originate from the v_6 resonance, 25% from the IMC, 23% from the 3:1 resonances, and 14% from the outer regions (OB and JFC). However, the Bottke et al. (2002a) model predicted about half of all NEAs have $a > 2$ AU, and our data mostly samples the $a < 2$ AU component of the NEA population, where the v_6 resonance and Mars Crossing regions dominate. Therefore, our model results are in agreement with the Bottke et al. (2002a) model.

The model results, presented as meteorite type vs. probable source region in Fig. 4, indicate that the v_6 secular resonance is the most probable source region for 75% of all NEAs with H, L, or LL chondrite mineralogies. NEAs with LL-chondrite mineralogies are more likely to be derived from the v_6 resonance than asteroids with H and L chondrites mineralogies (83% of LL chondrite-like NEAs compared to 57% of H and L chondrite-like NEAs). These results support the hypothesis that the Flora family, which lies near the v_6 resonance, is the source of the LL chondrites (Vernazza et al., 2008). It is not clear if our model results also support the suggestion that H chondrites are more likely to be derived from the 3:1

resonance (Thomas and Binzel, 2010). Model probabilities indicate that the NEAs with H chondrite mineralogies are more likely to be derived from the v_6 resonance (42%) than the Mars Crossing region (29%) or the 3:1 resonance (29%). However, almost all H-chondrite like NEAs have $a > 1.8$ AU and appear to reside in a distinct region of a, e, i space near the 3:1 resonance (Fig. 3). This is not what we would expect if the H and LL chondrite-like NEAs were both coming from the v_6 resonance. We plan to further investigate this issue in the near future.

Model results also suggest the NEAs with non-chondrite analogies (e.g. ureilites, primitive achondrites, basaltic achondrites, or olivine meteorites) are slightly less likely to be derived from the v_6 resonance than NEAs with ordinary chondrite mineralogies. Overall, 56% of the ureilites, basaltic achondrites, and olivine meteorites have a probable source near the v_6 resonance. The basaltic achondrites, however, are more likely to originate from the v_6 resonance than the other groups, with 63% having a probable source in near the v_6 resonance (Fig. 4). The Vesta family lies between the v_6 and 3:1 resonances, so we would expect asteroids with basaltic achondrite mineralogies to be derived from these regions. Because many objects in the 3:1 resonance are perturbed into Jupiter crossing orbits and ejected from the Solar System, the v_6 resonance is more efficient at creating short-lived near Earth objects ($a < 2$ AU) than the 3:1 resonance. Therefore, even if the Vesta family is sending an equal number of bodies into each resonance, the v_6 resonance would be the more probable source region for basaltic achondrites.

6. Summary

Previous studies on the diversity of the near-Earth asteroid population have relied primarily on modeling and statistical analysis to determine compositions. Here we determined the BARs and Band I centers of 72 m to km-sized NEAs and then derived the mineralogies of those NEAs with ordinary chondrite-like spectral parameters. Mineralogies, in terms of olivine and low-Ca pyroxene composition (mol% Fa and mol% Fs) and abundance (ol/(ol + px)), were used to determine the most probable ordinary chondrite analogue for each NEA. Finally, we determined the source region of these NEAs in order to look for potential correlations between size, composition, and source. From this study, we offer the following observations:

1. Of the 72 NEAs analyzed, 47 have spectral parameters that consistent with ordinary chondrites, overlap between ordinary chondrites and another meteorite, or plot in close proximity to the ordinary chondrite region. The remaining 25 have meteorite analogues other than ordinary chondrites or are not consistent with any known meteorite analogue.
2. Of the 47 NEAs with spectral parameters that plot within or near the ordinary chondrite region, 15% of these have H chondrite mineralogies, 10% have L chondrite mineralogies, 60% have LL chondrite mineralogies, and 15% have mineralogies that are either the L or LL chondrites.
3. Abundances of NEAs with ordinary chondrite mineralogies are consistent with results from previous studies, which indicate that the majority of NEAs have LL-chondrite mineralogies (Vernazza et al., 2008; de León et al., 2010). This, however, continues to be in conflict with the population of recovered ordinary chondrites, of which LL chondrites represent only 10%.
4. The size distribution and mineralogies of the NEAs that were classified as H, L, or LL chondrites are nearly identical for NEAs 1–10 km in diameter and NEAs < 1 km in diameter. This would appear to suggest that smaller bodies do not contribute material to planet-crossing orbits more readily than larger bodies.

However, our population of NEAs is biased towards those with visible and near-infrared spectra and represents a small percentage of total NEAs.

5. According to the source region model, 64% of NEAs are most likely to be derived from the ν_6 resonance, 20% from the Mars crossing region, 13% from the 3:1 resonance, and 3% from the outer belt region. NEAs with ordinary chondrites analogues, especially LL chondrites, appear to be preferentially derived from the ν_6 secular resonance, while NEAs with non-chondrite analogies are less likely to be derived from the ν_6 resonance.

6. Our results support the hypothesis that the Flora family, which lies near the ν_6 resonance, is the source of the LL chondrites (Vernazza et al., 2008).

Acknowledgments

Appendix A. Supplementary material

Supplementary data associated with this article can be found, in the online version, at http://dx.doi.org/10.1016/j.icarus.2012.11.007.

References

Abe, M., 2006. Near-infrared spectral results of asteroid Itokawa from the Hayabusa spacecraft. Science 312, 1334–1338.

Abell, P.A., Vilas, F., Jarvis, K.S., Gaffey, M.J., Kelley, M.S., 2007. Mineralogical composition of (25143) Itokawa 1998 SF36 from visible and near-infrared reflectance spectroscopy: Evidence for partial melting. Meteorit. Planet. Sci. 42, 2165–2177.

Adams, J.B., 1974. Visible and near-infrared diffuse reflectance spectra of pyroxenes as applied to remote sensing of solid objects in the Solar System. J. Geophys. Res. 79, 4829–4836.

Binzel, R.P., Xu, S., 1993. Chips off Asteroid 4 Vesta: Evidence for the parent body of basaltic achondrite meteorites. Science 260, 186–191.

Binzel, R.P., Bus, S.J., Burbine, T.H., Sunshine, J.M., 1996. Spectral properties of near-Earth asteroids: Evidence for sources of ordinary chondrite meteorites. Science 273, 946–948.

Binzel, R.P., Rivkin, A.S., Bus, S.J., Sunshine, J.M., Burbine, T.H., 2001. MUSES-C target Asteroid 1998 SF36: A reddened ordinary chondrite. Meteorit. Planet. Sci. 36, 1167–1172.

Binzel, R.P., Rivkin, A.S., Stuart, J.S., Harris, A.W., Bus, S.J., Burbine, T.H., 2004. Observed spectral properties of near-Earth objects: Results for population distribution, source regions, and space weathering processes. Icarus 170, 259–294.

Binzel, R.P., Thomas, C.A., DeMeo, F.E., Tokunaga, A., Rivkin, A.S., Bus, S.J., 2006. The MIT–Hawaii–IRTF joint campaign for NEO spectral reconnaissance. Lunar Planet. Sci. 37, 1491 (abstract).

Bottke Jr., W.F., Rubincam, D.P., Burns, J.A., 2000. Dynamical evolution of main belt meteroids: Numerical simulations incorporating planetary perturbations and Yarkovsky thermal forces. Science 145, 301–331.

Bottke Jr., W.F. et al., 2002a. Debiased orbital and absolute magnitude distribution of the near-Earth objects. Icarus 56, 399–433.

Bottke Jr., W.F., Vokrouhlický, D., Rubincam, D.P., Brož, M., 2002b. The effect of Yarkovsky thermal forces on the dynamical evolution of asteroids and meteoroids. In: Bottke, W.F., Cellino, A., Paolicchi, P., Binzel, R.P. (Eds.), Asteroids III. University of Arizona Press, Tucson, pp. 395–408.

Brearley, A.J., Jones, R.H., 1998. Chondritic meteorites. In: Papike, J.J. (Ed.), Planetary Materials, Reviews in Mineralogy. Mineralogical Society of America, Washington, DC, pp. 3-1–3-398.

Burbine, T.H. et al., 2001. Vesta, Vestoids, and the HEDs: Relationships and the origin of spectral differences. Meteorit. Planet. Sci. 36, 761–781.

Burbine, T.H., McCoy, T.J., Hinrichs, J.L., Lucey, P.G., 2006. Spectral properties of angrites. Meteorit. Planet. Sci. 41, 1139–1145.

Burbine, T.H., Buchanan, P.C., Dolkar, T., Binzel, R.P., 2009. Pyroxene mineralogies of near-Earth Vestoids. Meteorit. Planet. Sci. 44, 1331–1341.

Burns, R.C., Huggins, F.E., Abu-Eid, R.M., 1972. Polarized absorption spectra of single crystals of lunar pyroxene and olivine. Moon 4, 93–102.

Bus, S.J., 1999. Compositional Structure in the Asteroid Belt: Results of a Spectroscopic Study. M.S. Thesis, Massachusetts Institute of Technology, Boston, MA, USA.

Bus, S.J., Binzel, R.P., 2002a. Phase II of the small main-belt asteroid spectroscopic survey: The observations. Icarus 158, 106–145.

Bus, S.J., Binzel, R.P., 2002b. Phase II of the small main-belt asteroid spectroscopic survey: A feature-based taxonomy. Icarus 158, 146–177.

Chapman, C.R., 1996. S-type asteroids, ordinary chondrites, and space weathering: The evidence from Galileo's fly-bys of Gaspra and Ida. Meteorit. Planet. Sci. 31, 699–725.

Clark, B.E., Hapke, B., Pieters, C., Britt, D., 2002. Asteroid space weathering and regolith evolution. In: Bottke, W.F., Cellino, A., Paolicchi, P., Binzel, R.P. (Eds.), Asteroids III. University of Arizona Press, Tucson, pp. 169–182.

Cloutis, E.A., 1985. Interpretive Techniques for Reflectance Spectra of Mafic Silicates. M.S. Thesis, University of Hawaii, Honolulu, Hawaii, USA.

Cloutis, E.A., Gaffey, M.J., Jackowski, T.L., Reed, K.L., 1986. Calibrations of phase abundance, composition, and particle size distribution of olivine–orthopyroxene mixtures from reflectance spectra. J. Geophys. Res. 91, 11641–11653.

Cloutis, E.A. et al., 2010. Spectral reflectance properties of ureilites. Meteorit. Planet. Sci. 45, 1668–1694.

Cohen, M., Witteborn, F.C., Roush, T., Bregman, J., Wooden, D., 1998. Spectral irradiance calibration in the infrared. VIII. 5–14 micron spectroscopy of the asteroids Ceres, Vesta, and Pallas. Astron. J. 115, 1671–1679.

Consolmagno, G., Drake, M.J., 1977. Composition and evolution of the eucrite parent body: Evidence from rare Earth elements. Geochim. Cosmochim. Acta 41, 1271–1282.

de León, J., Licandro, J., Serra-Ricart, M., Pinilla-Alonso, N., Campins, H., 2010. Observations, compositional, and physical characterization of near-Earth and Mar-crosser asteroids from a spectroscopic survey. Astron. Astrophys. 517, A23. http://dx.doi.org/10.1051/0004-6361/200913852.

DeMeo, F.E., Binzel, R.P., Slivan, S.M., Bus, S.J., 2009. An extension of the Bus asteroid taxonomy into the near-infrared. Icarus 202, 160–180.

Drake, M.J., 2001. The eucrite/Vesta story. Meteorit. Planet. Sci. 36, 501–513.

Dunn, T.L., Cressey, G., McSween Jr., H.Y., McCoy, T.J., Bland, P.A., 2010a. Analysis of ordinary chondrites using powder X-ray diffraction: 1. Modal mineral abundances. Meteorit. Planet. Sci. 45, 123–134.

Dunn, T.L., McCoy, T.J., Sunshine, J.M., McSween Jr., H.Y., 2010b. A coordinated spectral, mineralogical, and compositional study of ordinary chondrites. Icarus 208, 789–797.

Gaffey, M.J., 2007. One pyroxene? Two pyroxenes? Three pyroxenes? Pyroxene compositions from asteroid spectra. Lunar Planet. Sci. 38, 1618 (abstract).

Gaffey, M.J. et al., 1993. Mineralogic variations within the S-type asteroid class. Icarus 106, 573–602.

Gaffey, M.J., Cloutis, E.A., Kelley, M.S., Reed, K.L., 2002. Mineralogy of asteroids. In: Bottke, W.F., Cellino, A., Paolicchi, P., Binzel, R.P. (Eds.), Asteroids III. University of Arizona Press, Tucson, pp. 183–204.

Gradie, J., Veverka, J., Buratti, B., 1980. The effects of scattering geometry on the spectrophotometric properties of powdered material. Proc. Lunar Planet. Sci. Conf. 11, 799–815.

Hapke, B., 2001. Space weathering from Mercury to the asteroid belt. J. Geophys. Res. 106, 10039–10074.

Hardersen, P.S., Gaffey, M.J., Abell, P.A., 2004. Mineralogy of Asteroid 1459 Magnya and implications for its origin. Icarus 167, 170–177.

Hardersen, P.S., Gaffey, M.J., Abell, P.A., 2005. Near-IR spectral evidence for the presence of iron-poor orthopyroxenes on the surfaces of six M-type asteroids. Icarus 175, 141–158.

Hardersen, P.S., Gaffey, M.J., Cloutis, E.A., Abell, P.A., Reddy, V., 2006. Near-infrared spectral observations and interpretations for S-asteroids 138 Tolosa, 306 Unitas, 346 Hermentaria, and 480 Hansa. Icarus 181, 94–106.

Harris, A.W., Harris, A.W., 1997. On the revision of radiometric albedos and diameters of asteroids. Icarus 126, 450–454.

Hartmann, W.K. et al., 1999. Reviewing the Yarkovsky effect: New light on the delivery of stone and iron meteorites from the asteroid belt. Meteorit. Planet. Sci. 34, A161–A167.

Hinrichs, J.L., Lucey, P.G., Robinson, M.S., Meibom, A., Krot, A.N., 1999. Implications of temperature-dependent near-IR spectral properties of common minerals and meteorites for the remote sensing of asteroids. Geophys. Res. Lett. 26, 1661–1664.

T.L. Dunn et al./Icarus 222 (2013) 273–282

Hiroi, T., Sasaki, S., 2001. Importance of space weathering simulation in compositional modeling of asteroids: 349 Dembowska and 446 Aeternitas as examples. Meteorit. Planet. Sci. 36, 1587–1596.

Hiroi, T., Takeda, H., 1991. Reflectance spectroscopy and mineralogy of primitive achondrites–lodranites. In: Proceedings of the NIPR Symposium on Antarctic Meteorites, vol. 4, pp. 163–177.

Hiroi, T. et al., 2006. Developing space weathering on the Asteroid 25143 Itokawa. Nature 443, 56–58.

Jarosewich, E., 1990. Chemical analyses of meteorites: A compilation of stony and iron meteorite analyses. Meteoritics 25, 323–337.

Jenniskens, P. et al., 2009. The impact and recovery of Asteroid 2008 TC3. Nature 458, 485–488.

Marchie, S., Brunetto, R., Magrin, S., Lazzarin, M., Gandolfi, D., 2005. Space weathering of near-Earth and main belt silicate-rich asteroids: Observations and ion experiments. Astron. Astrophys. 443, 769–775.

Mayne, R.G., McSween Jr., H.Y., McCoy, T.J., Gale, A., 2009. Petrology of the unbrecciated eucrites. Geochim. Cosmochim. Acta 73, 794–819.

McCoy, T.J., Nittler, L.R., Burbine, T.H., Trombka, J.I., Clark, P.E., Murphy, M.E., 2000. Anatomy of a partially differentiated asteroid: A "NEAR"-sighted view of acapulcoites and lodranites. Icarus 148, 29–36.

McCoy, T.J., Corrigan, C.M., Sunshine, J.M., Bus, S.J., Gale, A., 2007. Does spectroscopy provide evidence for widespread partial melting of asteroids?: II. Pyroxene compositions. Lunar Planet. Sci. 38, 1631 (abstract).

McFadden, L.A., Gaffey, M.J., McCord, T.N., 1985. Near-Earth asteroids – Possible sources from reflectance spectroscopy. Science 229, 160–163.

Mittlefehldt, D.W., McCoy, T.J., Goodrich, C.A., Kracher, A., 1998. Non-chondritic meteorites from asteroidal bodies. In: Papike, J.J. (Ed.), Reviews in Mineralogy, Planetary Materials, vol. 36. Mineralogical Society of America, Washington, pp. 4-1–4-195.

Moroz, L., Schade, U., Wäsch, R., 2000. Reflectance spectra of olivine–orthopyroxene-bearing assemblages at decreased temperatures: Implications for remote sensing of asteroids. Icarus 147, 79–93.

Nakamura, T. et al., 2011. Preliminary Examination of Hayabusa Asteroidal Samples: Mineralogy and Mineral-chemistry. Japan Geoscience Union Meeting (abstract).

Nesvorný, D., Vokrouhlický, D., Morbidelli, A., Bottke, W.F., 2009. Asteroidal source of L chondrite meteorites. Icarus 200, 698–701.

Okada, T. et al., 2006. X-ray fluorescence spectrometry of asteroid Itokawa by Hayabusa. Science 312, 1338–1341.

Pieters, C.M., Fischer, E.M., Rode, O., Basu, A., 1993. Optical effects of space weathering: The role of the finest fraction. J. Geophys. Res. 98, 20817–20824.

Pieters, C.M. et al., 2000. Space weathering on airless bodies: Resolving a mystery with lunar samples. Meteorit. Planet. Sci. 35, 1101–1107.

Rayner, J.T. et al., 2003. SpeX: A medium-resolution 0.8–5.5 micron spectrograph and imager for the NASA Infrared Telescope Facility. Publications of the Astronomical Society of the Pacific, vol. 115, pp. 362–382.

Reddy, V.A. et al., 2012c. Color and albedo heterogeneity of Vesta from Dawn. Science 336, 700–704.

Reddy, V., Gaffey, M.J., Kelley, M.S., Nathues, A., Li, J.-Y., Yarbrough, R., 2010. Compositional heterogeneity of Asteroid 4 Vesta's Southern Hemisphere: Implications for the Dawn Mission. Icarus 210, 693–706.

Reddy, V., Gaffey, M.J., Hardersen, P.S., 2012a. Constraining albedo, diameter and composition of near-Earth asteroid via near-IR spectroscopy. Icarus 219, 382–392.

Reddy, V. et al., 2012b. Photometric, spectral phase and temperature effects on Vesta and HED meteorites: Implications for Dawn Mission. Icarus 217, 153–168.

Roush, T.L., Singer, R.B., 1987. Possible temperature variations effects on the interpretation of spatially resolved reflectance observations of asteroid surfaces. Icarus 69, 571–574.

Rubincam, D.P., 1995. Asteroid orbit evolution and thermal drag. J. Geophys. Res. 100, 1584–1594.

Sanchez, J.A., Reddy, V., Nathues, A., Cloutis, E.A., Mann, Hiesinger, H., 2012. Phase reddening on near-Earth asteroids: Implications for mineralogical analysis, space weathering and taxonomic classification. Icarus 220, 36–50.

Sasaki, S., Nakamura, K., Hamabe, Y., Kurahashi, E., Hiroi, T., 2001. Production of iron nanoparticles by laser irradiation in a simulation of lunar-like space weathering. Nature 410, 555–557.

Singer, R.B., Roush, T.L., 1985. Effects of temperature on remotely sensed mineral absorption features. J. Geophys. Res. 90, 12434–12444.

Storm, S., Bus, S.J., Binzel, R.P., 2007. Olivine–pyroxene distribution of S-type asteroids in the main belt. Bull. Am. Astron. Soc. 39, 448 (abstract).

Sunshine, J.M., Pieters, C.M., Pratt, S.F., 1993. Deconvolution of mineral absorption bands – An improved approach. J. Geophys. Res. 95, 6955–6966.

Sunshine, J.M., Bus, S.J., McCoy, T.J., Burbine, T.H., Corrigan, C.M., Binzel, R.P., 2004. High-calcium pyroxene as an indicator of igneous differentiation in asteroids and meteorites. Meteorit. Planet. Sci. 39, 1343–1357.

Thomas, C.A. et al., 2011. ExploreNEOs. V. Average albedo by taxonomic complex in the near-Earth asteroid population. Astron. J., 142. http://dx.doi.org/10.1088/0004-6256/142/3/85.

Thomas, C.A., Binzel, R.P., 2010. Identifying meteorite source regions through near-Earth spectroscopy. Icarus 205, 419–429.

Thomas, P.H., Binzel, R.P., Gaffey, M.J., Storrs, A.D., Wells, E.N., Zellner, B.H., 1997. Impact excavation on Asteroid 4 Vesta: Hubble space telescope results. Science 277, 1492–1495.

Vernazza, P., Binzel, R.P., Thomas, C.A., DeMeo, F.E., Bus, S.J., Rivkin, A.S., Tokunaga, A.T., 2008. Compositional differences between meteorites and near-Earth asteroids. Nature 454, 858–860.

Xu, S., Binzel, R.P., Burbine, T.H., Bus, S.J., 1995. Small main-belt asteroid spectroscopic survey: Initial results. Icarus 115, 1–35.